Amide I Vibrational Dynamics of *N*-Methylacetamide in Polar Solvents: The Role of Electrostatic Interactions

M. F. DeCamp, L. DeFlores, J. M. McCracken, and A. Tokmakoff*

Department of Chemistry and George R. Harrison Spectroscopy Laboratory, Massachusetts Institute of Technology, Cambridge, Massachusetts 02139

K. Kwac and M. Cho*

Department of Chemistry and Center for Multidimensional Spectroscopy, Division of Chemistry and Molecular Engineering, Korea University, Seoul 136-701, Korea

Received: January 14, 2005; In Final Form: April 4, 2005

The vibrational frequency of the amide I transition of peptides is known to be sensitive to the strength of its hydrogen bonding interactions. In an effort to account for interactions with hydrogen bonding solvents in terms of electrostatics, we study the vibrational dynamics of the amide I coordinate of *N*-methylacetamide in prototypical polar solvents: D_2O, $CDCl_3$, and DMSO-d_6. These three solvents have varying hydrogen bonding strengths, and provide three distinct solvent environments for the amide group. The frequency−frequency correlation function, the orientational correlation function, and the vibrational relaxation rate of the amide I vibration in each solvent are retrieved by using three-pulse vibrational photon echoes, two-dimensional infrared spectroscopy, and pump−probe spectroscopy. Direct comparisons are made to molecular dynamics simulations. We find good quantitative agreement between the experimentally retrieved and simulated correlation functions over all time scales when the solute−solvent interactions are determined from the electrostatic potential between the solvent and the atomic sites of the amide group.

I. Introduction

The spectroscopy of the amide group forms the basis for understanding much of the infrared (IR) spectroscopy of proteins and peptides. In particular, the amide I absorption band of protein backbones is sensitive to conformation in the way it reflects vibrational couplings and hydrogen bonding to the amide group.[1−4] A large number of investigations have developed relationships between amide I vibrational couplings and peptide or protein conformation, and more recently, peptide conformational dynamics encoded in time-dependent fluctuations of the couplings have been characterized.[5−8] Less attention has been paid to the influence of hydrogen bonding, although it plays a fundamental role in describing protein and peptide vibrational spectra in solution.[9−15] Recent femtosecond IR experiments[4,16−18] and molecular dynamics simulations[19,20] have begun to explore the nature of solute−solvent interactions on amide I vibrational dynamics, focusing on the model compound for a single peptide unit, *N*-methylacetamide (NMA).

To gain more molecular insight into the influence of hydrogen bonding and solvent−solvent interaction on fluctuations of amide I energies, we have chosen to study the amide I vibrational frequency fluctuations of NMA in different polar solvents using femtosecond IR spectroscopy. The study of the vibrational dephasing of NMA in solvents of varying polarity and hydrogen bonding character allows for a systematic study of the influence of solvent electrostatics and hydrogen bonding on the vibrational dynamics. NMA has been widely studied, and recently its amide I vibrational dynamics have been the object of experiments and simulation. The amide I vibration is composed primarily of a C═O stretch coupled with a small N−H deformation. Both IR absorption spectroscopy and molecular dynamics simulations have demonstrated that the frequency response of this vibration is very sensitive to the hydrogen bonding to the C═O group.[14,19−21] It has also been shown that vibration is also sensitive to the number of hydrogen bonds and the hydrogen bonding geometry. In particular, an empirical formula describing the red shift of the amide I band due to hydrogen bonding has been proposed:[4]

$$\delta\bar{\nu} = \alpha\{2.6 - r_{O\cdots H}\} \qquad (1)$$

where α is a proportionality constant (typically -30 cm^{-1}/Å), $r_{O\cdots H}$ (Å) is the hydrogen bonding distance between the oxygen of the peptide bond and the nearest hydrogen, and $\delta\bar{\nu}$ is the observed frequency shift from the gas phase. A similar relationship correlates the amide I vibrational energy with the hydrogen bonding strength to the peptide group.[22]

Geometrical relationships between amide I frequency and hydrogen bonding are appealing in terms of a structure−frequency correlation, but such observations raise further questions. In particular, can the role of hydrogen bonding in the vibrational spectroscopy of proteins be more accurately and generally described as a simple electrostatic interaction? There is increasing evidence, based on studies of aqueous solutes,[23−27] peptides,[19,20,28] and proteins,[29,30] that vibrational dephasing in hydrogen bonding solution is well described when interactions with the surrounding environment are accounted for purely through an electrostatic model. Specifically for the case of NMA, a linear correlation between the electrostatic potential of the hydrogen bonding solvent and the amide I frequency of the solute NMA has been combined with molecular dynamics simulations to accurately predict the experimental red shift and dynamics of the amide I vibration.[19] Additionally, studies have

10.1021/jp050257p CCC: $30.25
Published on Web 05/07/2005

made comparisons of how the electrostatic potential at the amide I atomic sites and the electric field acting on the amide I coordinate correlate with the amide I frequency.[31−33] Electrostatic interactions are the dominant forces that a polar solvent can exert on a vibrational coordinate, which influence both the vibrational frequency fluctuations and vibrational lifetime. These predictions imply that the electric field fluctuations of the solvent will dictate most of the observed frequency dynamics.[26] We can characterize the frequency−frequency correlation function,

$$C(t) = \langle \delta\omega(t)\delta\omega(0)\rangle \qquad (2)$$

which reveals the loss of "memory" of an isolated vibrational mode due to time-dependent fluctuations in the amide I frequency $\delta\omega(t)$. Nonlinear-IR spectroscopy of the amide I band can be modeled to obtain $C(t)$ and other dynamical quantities. As NMA involves a single amide group, there has been considerable interest in measuring the frequency response of the amide I band of NMA and other peptides in various solvent environments.[16−20,28,34−38]

Multidimensional IR spectroscopic techniques are sensitive to vibrational interactions of molecular systems. In particular, three-pulse stimulated photon echo (3PE) and time-resolved two-dimensional Fourier transform infrared spectroscopy (2D IR) have been used to determine the dynamics on a number of systems including hydrogen bonding networks in water[26,39−41] and peptides.[3,16,18−20,42] 3PE and 2D IR spectroscopy are both femtosecond third-order nonlinear techniques, whereby three resonant ultrafast pulses are used to create a vibrational echo. The temporal separation of the first two pulses (τ_1) creates a frequency grating, which is mapped onto the distribution of vibrational frequencies within the vibrational resonance. Following a variable waiting time τ_2, the final pulse scatters off the material frequency grating creating an echo signal. 3PE methods characterize the scattered intensity as a function of τ_1, whereas 2D IR spectroscopy heterodyne detects the shape of the radiated echo signal during a detection period τ_3 for all values of τ_1. The Fourier transform of these variables is a 2D IR correlation spectrum that is related to the joint probability that excitation of a frequency ω_1 will be detected at ω_3 following the waiting time.

The shape, position, and time dependence of the 3PE and 2D IR have distinctive signs of the vibrational dynamics. The echo signal as a function of τ_2 reveals the vibrational dynamics of the system including the "memory" of the initial frequency grating (via the 3PE profile) and the vibrational lifetime (via the scattering amplitude). In particular, the temporal maximum (the so-called "peak shift") and asymmetry of the 3PE signal reflects the effect of the inhomogeneous broadening.[34,43−45] Vibrational broadening is reflected in the 2D IR experiment by the shape and relative slope of the 2D line shapes;[19,46] diagonal elongation of the absorption resonance indicates inhomogeneous broadening whereas symmetric line shapes indicate homogeneous broadening. In addition, dispersing the spectrum along two dimensions provides the means of observing vibrational transitions otherwise hidden in traditional 1D spectroscopy as well as observing vibrational couplings via appearance of cross-peaks.[47,48] The combination of 1D spectroscopies with multidimensional spectroscopies can provide a method of isolating the vibrational dynamics of solvated compounds.

Changes in the frequency−frequency correlation function under the influence of different hydrogen bonding interactions yield information on the dynamics of the amide I vibration. The primary goal of this paper is to deduce whether electrostatics fluctuations are the primary influence on the vibrational dynamics and to compare experimental results to molecular dynamics simulations to obtain structural information of the hydrogen bonding associated with solvation. Here we perform stimulated 3PE, 2DIR, and transient pump−probe spectroscopy to extract $C(t)$ for NMA in heavy water (D_2O), chloroform ($CDCl_3$), and dimethyl sulfoxide (DMSO-d_6). The combination of experimental techniques allows the effects of vibrational dephasing, population relaxation, and reorientation to be separated.

These three solvents represent model hydrogen bonding interactions with the amide vibration: D_2O is a medium-to-strong hydrogen bond donor and acceptor for the peptide group (making up to two hydrogen bonds to C═O and accepting one from the N−H), while $CDCl_3$ (hydrogen bond donor) and DMSO-d_6 (hydrogen bond acceptor from the N−H) interact weakly with the amide group. Furthermore, these solvents differ in the time scale of their intermolecular motions. Although some of these solvents are not traditionally thought of as hydrogen bonding, we justify these assignments on the basis of geometrical criteria in molecular dynamics simulations. Additional comparisons to molecular dynamics simulations provide insight into the nature of the dynamics of the peptide group. We demonstrate that the treatment of the amide I vibrational solvation dynamics in these polar solvents is accurately described by the electrostatic interactions between the amide I coordinate and the fluctuating configurations of charges in the solvent.

II. Methods

A. Experimental Details. The design of the experimental system has been described in detail elsewhere[47] and will only be discussed briefly here. An ultrafast 800 nm, 1 kHz laser system pumps a commercial OPA which produces ~1 μJ, 90 fs mid-IR pulses. The OPA was tuned to be resonant with the amide I transition of NMA (~6 μm). The Fourier transform bandwidth of the laser pulses (~150 cm^{-1}) spans the fundamental ($v = 0 \rightarrow 1$) and overtone ($v = 1 \rightarrow 2$) transitions of NMA such that the IR pulse can be treated as a δ function in time.

Polarization-sensitive pump−probe measurements of the amide I vibration were taken with wire grid polarizers to control the polarization. Three standard polarization geometries were used: parallel ($S_{\parallel}$), perpendicular ($S_{\perp}$), and magic angle (S_{MA}). The transmitted probe pulse was dispersed in a monochromator centered on the $v = 0 \rightarrow 1$ transition and collected with a liquid nitrogen cooled MCT detector. A third reference beam was simultaneously dispersed and its intensity collected on a separate detector. The resultant integrated reference and probe pulses are divided using an analogue math processor for shot normalization purposes. The pump beam was chopped at 500 Hz, and a lock-in amplifier collected the modulated signal. The pump−probe anisotropy was determined from $r(t) = (S_{\parallel} - S_{\perp})/(S_{\parallel} + 2S_{\perp})$.

For the 3PE and 2D IR spectroscopy, three IR pulses (denoted by their wavevectors $\vec{k}_a$, $\vec{k}_b$ and $\vec{k}_c$) are focused in the boxcar geometry resulting in a third-order nonlinear signal (E_{sig}) emitted in the phase-matched direction, $\vec{k}_{sig} = -\vec{k}_a + \vec{k}_b + \vec{k}_c$. The polarizations of each of the fields were parallel. The time delays between consecutive pulses are τ_1 and τ_2, and the time period following the final pulse during which the signal is radiated is τ_3. We acquire two distinct signals which differ by the time-ordering of the optical pulses along the incident wave vectors: rephasing ($\vec{k}_{sig} = -\vec{k}_1 + \vec{k}_2 + \vec{k}_3$) and nonrephasing ($\vec{k}_{sig} = +\vec{k}_1 - \vec{k}_2 + \vec{k}_3$).

For 3PE measurements, the signal was collected by a liquid nitrogen cooled MCT detector. For fixed waiting times, τ_2, the

3PE intensity was measured as a function of τ_1 revealing the integrated echo profile. Much like the traditional echo peak shift measurement,[49] we acquire both rephasing and nonrephasing signals, displaying rephasing signals for positive τ_1 and nonrephasing signals for negative τ_1.

For the 2D IR measurements, the signal was spatially and temporally overlapped with a local oscillator pulse for heterodyne detection. The heterodyned signal was collected by a 64-channel liquid nitrogen cooled MCT array detector. One of the input beams is chopped at 500 Hz, leading to a modulated detection intensity. The difference signal gives the interference between signal and local oscillator, which was observed at all detection frequencies ω_3 as a function of τ_1. To generate a 2D IR correlation spectrum, rephasing and nonrephasing signals are acquired and Fourier transformed. The real part of the rephasing and nonrephasing spectra are summed to obtain a 2D absorptive line shape.[47] We use the phasing method described in ref 50.

Undueterated *N*-methylacetamide ($CH_3(CONH)CH_3$; NMA) was purchased from Aldrich and used without further purification. Fully deuterated solvents D_2O, DMSO-d_6, $CDCl_3$, and CD_3OD (MeOD) were acquired from Cambridge Isotope Labs and used as received. Solutions in each of the solvents were at a concentration of 10 mg/mL. The labile N-bonded hydrogen of NMA exchanges with deuterium in the protic solvents to give $CH_3(COND)CH_3$ (NMA-*d*). The sample was then placed between two CaF_2 windows spaced 50 μm apart. All experiments were performed at room temperature. No change in the IR absorption spectrum was observed over the course of the data acquisition.

B. Modeling the Data. We obtain the amide I frequency correlation function by self-consistently modeling the pump−probe and 3PE data with a nonlinear response function that accounts for vibrational frequency fluctuations, molecular reorientation, and vibrational population lifetime.[39] Construction of the response function is described in detail elsewhere[39,47] and is summarized briefly here. 3PE experiments constrain $C(t)$, while magic angle pump−probe and pump−probe anisotropy measurements constrain the amide I population and orientational relaxation. Similar approaches to modeling 3PE data have been described by others.[5,51]

In the limit of short pulse duration, the radiated signal is proportional to the nonlinear response function $\bar{R}^{(3)}$. $\bar{R}^{(3)}$ is calculated by summing over all possible Liouville pathways that contribute to either the rephasing or nonrephasing experiments.[47] When vibrational and orientational motion is decoupled, $\bar{R}^{(3)}$ can be written as a product of the response function for vibrational frequency fluctuations R, the population relaxation of the nonlinear polarization Γ, and the amide I orientational response function Y:[39]

$$\bar{R}^{(3)}(t_3,t_2,t_1) = R(t_3,t_2,t_1)\Gamma(t_3,t_2,t_1)Y(t_3,t_2,t_1) \qquad (3)$$

The vibrational dephasing dynamics described by R was calculated as described by Sung and Silbey[52] and Cho.[53] It was assumed the amide I vibration was a simple three-level system with an anharmonicity of $\omega_{10} - \omega_{21} = 16\ \mathrm{cm}^{-1}$. It was further assumed that $C(t)$ can be accurately modeled as a multiexponential function:

$$C(t) = \sum_n \Delta_n^{\,2} \exp(-t/\tau_{c,n}) \qquad (4)$$

$C(t)$ characterizes the fluctuations of the fundamental transition frequency $\delta\omega_{10}(t)$, and was related to correlation functions for the fluctuations of vibrational energy gaps involving $v = 2$ by harmonic scaling relations.[47]

Vibrational population relaxation was also taken into account such that the relative amplitude and shape of 3PE profiles could be fit simultaneously with the dispersed pump−probe signal, using the same nonlinear response formalism. To incorporate the vibrational lifetime into the calculation, we used a biexponential form

$$\Gamma(t_1,t_2,t_3) = \sum_m B_m \exp(-\gamma_m(t_1+t_3)/2 - \gamma_m t_2) \qquad (5)$$

where $1/\gamma_m$ and B_m are the measured population relaxation rate and amplitude of the nth component, respectively, obtained from a fit to the magic angle pump−probe data.

The orientational response function, Y, depends on the polarization of the incident fields and the reorientational motion of the amide I transition dipole. For this model we assume that the molecule can be treated as spherical rotors and that all the transition moments lay along the same molecular axis. For isotropic orientational diffusion, the tensor can be written as:[54]

$$Y_{ZZZZ} = \frac{1}{9}p_1(t_1)p_1(t_3)\left(1 + \frac{4}{5}p_2(t_2)\right) \qquad (6)$$

$$Y_{ZZYY} = \frac{1}{9}p_1(t_1)p_1(t_3)\left(1 - \frac{2}{5}p_2(t_2)\right) \qquad (7)$$

Here the ith-order Legendre polynomial reorientation correlation functions for the transition dipole unit vectors are $p_i(t) = \langle P_i(\hat{\mu}(t)\cdot\langle\hat{\mu}(0)\rangle)\rangle$. Y_{ZZZZ} applies to $S_{\|}$, Y_{ZZYY} applies to $S_{\perp}$, and S_{MA} is described by $(Y_{ZZZZ} + 2Y_{ZZYY})/3$. From the form of the anisotropy measurements, we fit the orientational correlation function to biexponentials $p_2(t) = S_1 e^{-t/\tau_{or,1}} + S_2 e^{-t/\tau_{or,2}}$. In modeling, we also use the diffusive scaling relationship $p_1(t) = p_2(t/3)$.

C. Simulation. To directly compare the numerical simulation results with experiments, we performed molecular dynamics (MD) simulations of NMA in D_2O, DMSO, and $CDCl_3$ using the SANDER module of the AMBER program package[55] employing the parm99 force field.[55,56] 387 D_2O molecules, 151 DMSO molecules, and 278 $CDCl_3$ molecules are used to solvate a single NMA molecule for the NMA−D_2O, NMA−DMSO, and NMA−$CDCl_3$ systems, respectively. Each system is in a cubic box under a periodic boundary condition. Long-range electrostatic interactions are treated by the particle-mesh Ewald method[57] implemented in AMBER. Each system is minimized by 1000 steps of the conjugate gradient method, and then is equilibrated for 200 ps at 298 K with use of the Berendsen coupling algorithm.[58] The final configurations obtained by this procedure are used as input for the production run of 4 ns constant-energy MD. A time step of 0.5 fs is used for both the equilibration and production runs. For the NMA−methanol system, we used the MD trajectory obtained from the previous work in ref 20.

Trajectories in the various solvents were used to calculate the frequency correlation function and the reorientational correlation function. $C(t)$ was calculated by using the amide I mode frequency shift determined from snapshot configurations of the MD trajectories for the NMA solvated in D_2O, DMSO, and $CDCl_3$. The amide I frequency shift is determined from the recently proposed empirical formula that correlates ω with the electrostatic potential originating from the solvent and acting on the atomic sites of NMA, ϕ_a:[14,19]

$$\delta\omega(t) = 2\pi c\sum_a l_a\phi_a(t) \qquad (8)$$

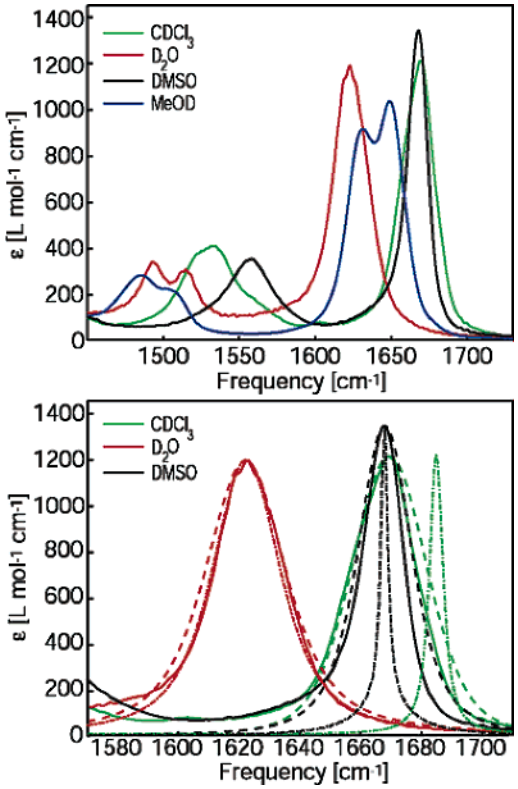

Figure 1. (a) FTIR absorption spectra of NMA in the amide I and amide II regions. Solvents: $CDCl_3$ (green, 1669 cm^{-1}), D_2O (red, 1622 cm^{-1}), DMSO-d_6 (black, 1668 cm^{-1}), and MeOD (blue, 1631 and 1649 cm^{-1}). (b) Fits to FTIR amide I line shapes. Solid lines are the measured spectra, dashed lines are calculated line shapes from the retrieved correlation function, using eq 10, and dotted lines are those line shapes predicted from molecular dynamics simulation.

Here ϕ_a are calculated from the solvent partial charges (from the TIP3P water model) and the correlation parameters for the individual NMA sites l_a were determined from ab initio calculations and are given in ref 14. The reorientational correlation function $p_2(t)$ is also obtained from MD trajectories by using the time-varying angle between the amide I transition dipole vectors.

III. Results

A. IR Absorption Spectra. Infrared absorption spectra of NMA in the various solvents, shown in Figure 1 for the amide I and amide II transitions, hints at the differing hydrogen bonding interactions to the amide group. The large red shift from the gas phase[59] (~100 cm^{-1}) as well as the broad line shape (~35 cm^{-1}) observed in D_2O indicates that water has strong hydrogen bonding interactions with the amide group. This is attributed to the existence of three hydrogen bonding sites to the NMA in water: two to the oxygen and one from the hydrogen.[60] The NMA/D_2O spectrum differs noticeably from the absorption spectra in DMSO and $CDCl_3$, which are less red shifted and much narrower, indicating weaker hydrogen bonding.[12,14,19,21] While apparently weakly interacting, the amide I band of NMA in $CDCl_3$ appears asymmetric, indicating vibrational substructure within the amide I region. The amide I spectrum in MeOD shows a very different two-peak structure that lies intermediate to D_2O and the aprotic solvents. The two-peak structure is attributed to NMA species with either one or two hydrogen bonds from MeOD.[16,20]

An additional difference between the spectroscopy of the solvents is the protonation state of the amide hydrogen. The polar protic solvents rapidly exchange hydrogens with NMA giving $CH_3(COND)CH_3$ (NMA-*d*), and the vibration of interest is properly termed amide I′. This deuteration also leads to a two-component structure in the amide II region, which has previously been attributed to a mixing of the amide II′ vibration with the methyl-d_3 umbrella distortion to produce two bands with CH bend and CN stretch character.[59]

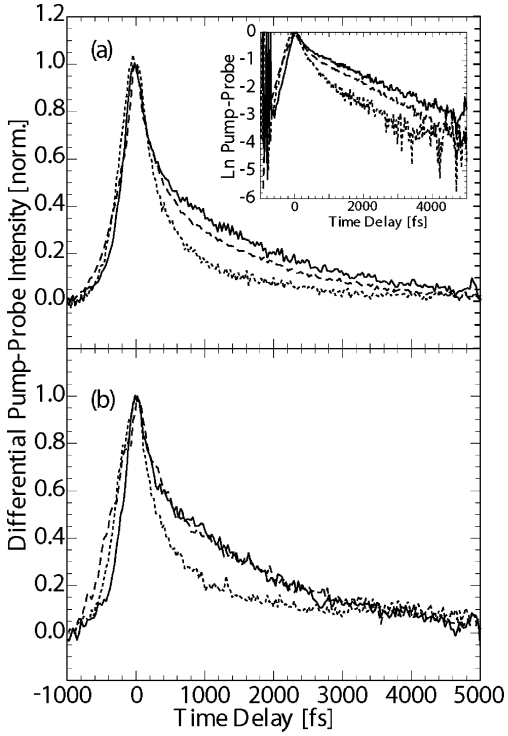

Figure 2. (a) Parallel pump−probe signals ($S_{||}$) of NMA in D_2O (dotted), DMSO-d_6 (dashed), and $CDCl_3$ (solid). Inset: Semilog plot of $S_{||}$. (b) Magic angle pump−probe (S_{MA}). All pump−probe signals were dispersed and detected at the peak of the $v = 1 \rightarrow 0$ amide I transition.

In the case of the polar aprotic solvents, no hydrogen exchange is present, and the dominant NMA species in solution is $CH_3(CONH)CH_3$. This is seen from the single peak amide II transitions that are blue shifted as a result of protonation in $CDCl_3$ and DMSO. Also for the case of $CDCl_3$, the presence of a free NH peak (3465 cm^{-1}, not shown) indicates no hydrogen exchange and no hydrogen bonding of the NH to the solvent. A lower frequency shoulder is observed at 3340 cm^{-1}, which might seem to suggest that N−H hydrogen bonding is present. We rule out the presence of NMA dimers[61] since this band intensity scales linearly with NMA concentration and rule out the presence of water in the solvent from its IR spectrum. Rather we adopt the earlier assignment to the Amide B transition (combination bands and overtones intensified by Fermi resonance).[12]

B. Femtosecond IR Spectroscopy. Time-resolved dispersed pump−probes of the NMA amide I band in the three solvents (see Figure 2) display distinct differences in the relaxation behavior. Qualitative comparison makes it clear that the vibrational relaxation dynamics in D_2O is much faster than that in the other solvents. The log of the signals reveals a distinct biexponential behavior in the amide I relaxation in all three solvents (Figure 2 inset) with a separation into two characteristic time scales: a 150−300 fs fast relaxation and a relatively slow picosecond component. Pump−probe measurements taken in the magic angle geometry are independent of NMA reorientational motion and reveal nonexponential vibrational population

TABLE 1: Biexponential Fit Parameters for the Pump−Probe and Anisotropy Measurements $\Delta T(t) = B_1 e^{-\gamma_1 t} + B_2 e^{-\gamma_2 t}$

solvent	pol.	B_1	$1/\gamma_1$ [fs]	B_2	$1/\gamma_2$ [fs]
D_2O	magic	0.55	202 ± 25	0.45	857 ± 87
	anisotropy (exptl)	0.1	186	0.33	9800 ± 8700
	anisotropy (MD)	0.09	209	0.32	4306
DMSO-d_6	magic	0.43	257 ± 22	0.67	2324 ± 170
	anisotropy (exptl)	0.07	295 ± 160	0.345	16000 ± 4500
	anisotropy (MD)	0.07	295	0.32	12830
$CDCl_3$	magic	0.33	140 ± 19	0.73	1860 ± 90
	anisotropy (exptl)	0.07	220 ± 160	0.30	9500 ± 2900
	anisotropy (MD)	0.11	297	0.29	5858

relaxation. S_{MA} of each of the solvents can be accurately fit to a double exponential, as summarized in Table 1. The pump−probe signal detected at the peak of the $v = 1 \rightarrow 2$ induced absorption gives approximately the same decay with a slight variation in time scales. This form of the decay reveals the vibrational relaxation from the amide I $v = 1$ state is not a simple two-state process. Previous measurements of T_1 for NMA/D_2O with 180 fs pulses reported biexponential relaxation with time constants of 450 fs and 4 ps.[34]

Figure 3 shows the experimental anisotropy obtained from $S_{\parallel}$ and $S_{\perp}$ pump−probe measurements, together with fits. Taking into account that $r(0) = 0.4$, the data are best described by a biexponential consisting of a low amplitude <300 fs component and a several-picosecond decay. This separation of time scales argues that the short time behavior involves librational motion of the NMA and/or solvent, and the picosecond tail is diffusive molecular reorientation. In Figure 3 we also compare the experimental anisotropy decay with the reorientational correlation function obtained from MD trajectories. The MD results are in good agreement with experiment, showing similar fast and slow components of roughly the same amplitudes. Our data for longer times corresponds to the 6 ps decay reported by Hamm.[34]

Time-dependent 3PE profiles of NMA in the various solvents for a series of waiting times (τ_2) are shown in Figure 4. The temporal profile of the integrated 3PE in D_2O (Figure 4a) shows similar features to that reported by Zanni et al.:[18] the quasitriangular intensity profile, the echo peak centered around $\tau_1 = 0$, and a temporal width of ~400 fs. The lack of an echo peak shift implies that the transition is not inhomogeneously broadened. Even over a period of 200 fs, a period shorter than the inverse of the amide I line width, there is rapid averaging of the amide I frequency, which is consistent with the fast time scale of intermolecular librational and translational motions in D_2O. However, some residual slow dynamics do act on the amide I transition, as observed through the asymmetry of the 3PE signal about $\tau_1 = 0$. This inhomogeneity is also seen through the diagonal elongation of the 2D IR spectra of NMA:D_2O (see Figure 5a). For waiting times less than 1 ps, the 2D line shapes show a clear diagonal tilt characteristic of inhomogeneous broadening. This tilt can be visualized through the slope of the node between the positive and negative resonances. At longer waiting times the transition relaxes back to the homogeneous limit.

As the electrostatic interactions between NMA and the surrounding solvent become weaker and the time scale for solvent relaxation slows, significant changes are evident in the 3PE signal and the 2D IR surfaces. The 3PE data of NMA solvated by DMSO-d_6 and $CDCl_3$ (Figure 4b,c) display a Gaussian-like echo profile with a temporal width of ~700 fs while the peak of the 3PE signal is shifted by ~200 fs from $\tau_1 = 0$. The larger echo width is consistent with the longer dephasing time and the large echo peak shift is representative of significant inhomogeneity on the time scale of the measurement. Similar conclusions can be drawn from the 2D IR amide I spectra in these solvents. Even though the absorption line is much narrower than in D_2O, the 2D IR surfaces for solvation in DMSO-d_6 (Figure 5b) show the vibration remains inhomogeneously broadened well beyond 1 ps. Solvation by $CDCl_3$ displays a more unusual response. The 2D IR line shapes show significant diagonal elongatation, even after long waiting times (>6 ps). Yet, for waiting times >3 ps the 2D line shape appears to be asymmetric on either side of the resonance. The slope of the node between positive and negative peaks varies from diagonal on the red side of the line center to horizontal on the blue side. This observation indicates a heterogeneous dynamics for the amide I solvation by chloroform, which originates in the coordination between NMA and $CDCl_3$. Since blue shifts are associated with weaker hydrogen bonding interactions, it seems likely that weaker solute−solvent interactions are also associated with more rapid local solvent fluctuations. This asymmetric line shape may in fact imply that the broad absorption line of NMA:$CDCl_3$ originates from a distribution of solvation species that exchange on picosecond time scales, analogous to what has been discussed for NMA solvated in MeOD.

For NMA:MeOD two distinct amide I vibrational resonances are seen (see Figure 1) corresponding to one or two hydrogen bound solvent molecules.[16,20] In Figure 6a we show the 2D IR amide I spectra of NMA-*d*:MeOD. For early waiting times these spectra show two distinct diagonally elongated resonances. Over the course of 5 ps, the line shapes gradually homogenize and off-diagonal amplitude between the two resonances grows in giving a measure of the kinetics for hydrogen bond forming and breaking. Our observations are consistent with those made previously by Hamm and co-workers using double resonance 2D IR measurements.[16]

C. Correlation Functions. The self-consistent modeling of the nonlinear-IR experiments described in Section IIB was used to obtain the frequency correlation function for the solvents with one resolved amide I resonance: D_2O, $CDCl_3$, and DMSO-d_6. Polarization-selective pump−probe experiments constrained the population relaxation and reorientation with relatively little influence from the dephasing described by $C(t)$. The 3PE profiles and peak shift are most sensitive to $C(t)$,[49,62] although their relative amplitudes as a function of τ_2 reflect population and orientational relaxation. Due to the lack of peak shift in the water data and the non-Gaussian echo profile, we fit the τ_1 and τ_2 dependent 3PE amplitude and profile to extract $C(t)$. Since the 3PE peak shift and rotation of the 2D line shape with τ_2 reflect the slow relaxation of correlations, the time scales for this relaxation were used as an initial guess for the long component of $C(t)$ in eq 4 (approximately 1, 3, and 6 ps for D_2O, DMSO-d_6, and $CDCl_3$, respectively). In the fitting routine, the extracted lifetime and anisotropy were held fixed, while the amplitude and decay of the multiexponential correlation function were floating variables.

As a final constraint, the retrieved correlation function was used to calculate the IR absorption line shape and then compared directly with the measured FTIR line width (see Figure 1). It was assumed that the vibrational frequency fluctuations followed Gaussian statistics such that the absorption line width could be calculated directly from the retrieved vibrational correlation function

$$I(\omega) = \int_{-\infty}^{\infty} e^{i(\omega-\omega_{10})t-g(t)} p_1(t)\Gamma(t)\, dt \qquad (9)$$

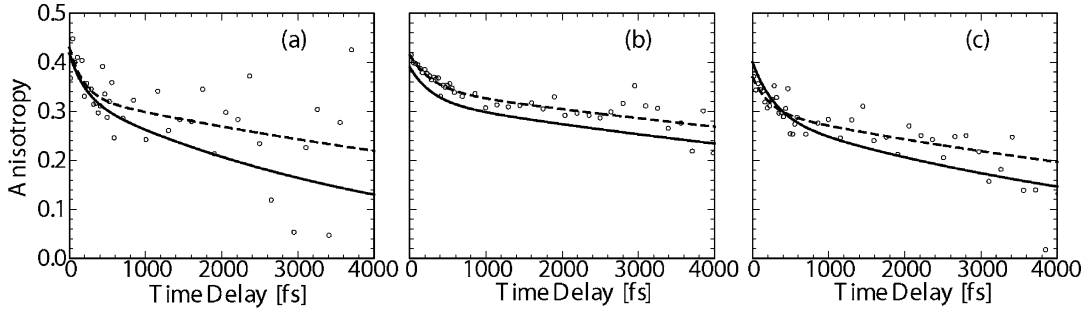

Figure 3. Measured anisotropy $r(t)$ for (a) D_2O (b) DMSO-d_6, and (c) $CDCl_3$. Dashed lines are a biexponential fit with coefficients listed in Table 1 and solid lines are calculated from MD trajectories.

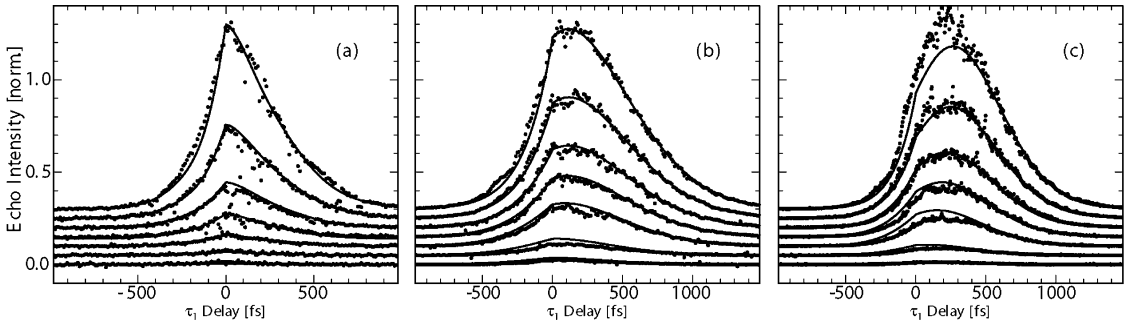

Figure 4. Integrated three pulse echo profiles $I_{3PE}(\tau_1)$ of NMA in (a) D_2O, (b) DMSO-d_6, and (c) $CDCl_3$. Waiting times of $\tau_2 = 150$, 300, 500, 700, 1000, 2000, and 3000 fs are shown on each plot from top to bottom. The black points indicate the measured echo and the solid line is the retrieved fit.

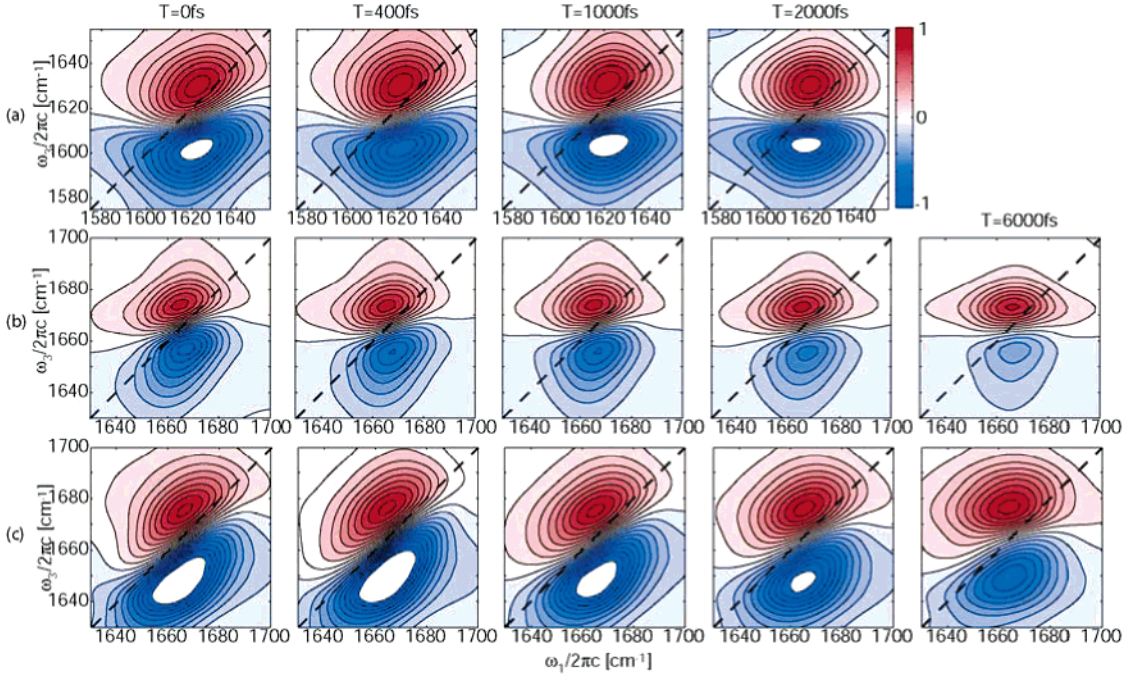

Figure 5. 2D IR line shapes of NMA in the three solvents for varying waiting times. (a) D_2O for $\tau_2 = 0$, 400, 1000, and 2000 fs (left to right). Individual spectra are normalized to the peak of the fundamental transition and plotted in 10% contours. (b) DMSO-d_6 and (c) $CDCl_3$ for $\tau_2 = 0$, 400, 1000, 2000, and 6000 fs.

where

$$g(t) = \int_0^t dt_1 \int_0^{t_1} dt_2 \langle \delta\omega(t_1)\delta\omega(t_2)\rangle \qquad (10)$$

and the vibrational lifetime decay $\Gamma(t) \equiv \Gamma(t,0,0)$ as defined in eq 5.

Fits to the 3PE data from this modeling for NMA solvated in D_2O, DMSO, and $CDCl_3$ are shown in Figure 4. Also, the absorption line shapes in these solvents obtained from eqs 9 and 10 are shown in Figure 1b. These show that our response function works quite well to capture the amplitude and shape of the 3PE data as well as the polarization-dependent pump−probe measurements, and gives reasonable agreement for the line shapes.

The extracted correlation functions for the three solvents are plotted in Figure 7 and summarized in Table 2. In each case, we find that both femtosecond and picosecond relaxation processes are present in $C(t)$. In the case of D_2O the behavior

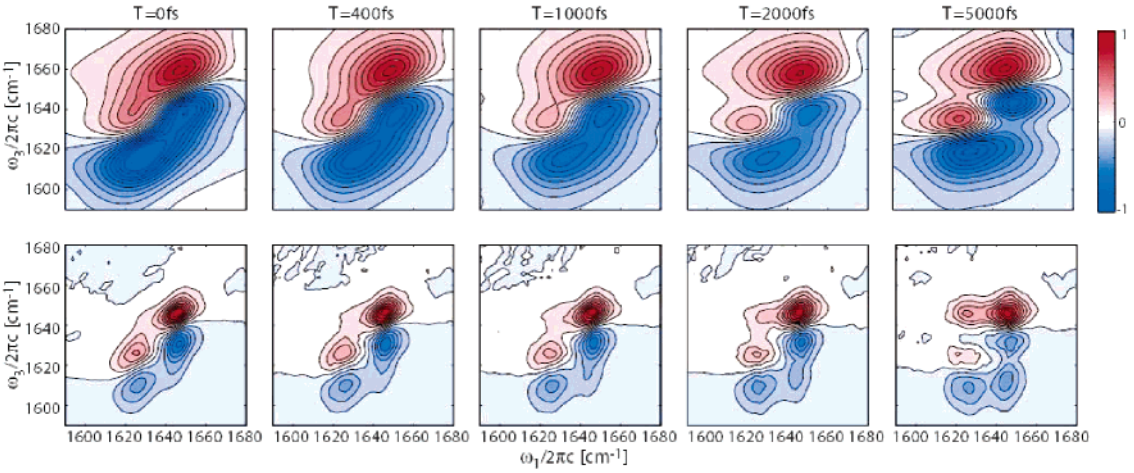

Figure 6. (a) Experimental 2D IR amide I spectra of NMA in MeOD. The double peak structure is indicative of singly and doubly hydrogen bound solvent molecules. Individual spectra are normalized to the peak of the fundamental transition and plotted in 10% contours. (b) 2D IR spectra of NMA in MeOH obtained from simulation.[20]

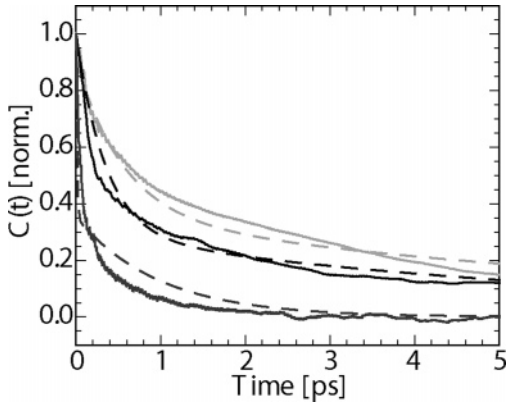

Figure 7. Retrieved (dashed) and calculated (solid) correlation functions for NMA in D_2O (dark gray), DMSO-d_6 (black), and $CDCl_3$ (light gray).

TABLE 2: Extracted Frequency−Frequency Correlation Functions for Different Solvents[a]

solvent		Δ_1 [ps^{-1}]	$\tau_{c,1}$ [fs]	Δ_2 [ps^{-1}]	$\tau_{c,2}$ [fs]	Δ_3 [ps^{-1}]	$\tau_{c,3}$ [fs]
D_2O	(fit)	3.0	10			2.2	980
	(sim.)	2.6	56			1.7	660
DMSO-d_6	(fit)	0.9	52	1.4	330	1.4	2800
	(sim.)			1.4	347	0.9	6200
$CDCl_3$	(fit)	0.6	4	1.9	620	1.6	5600
	(sim.)			1.0	256	1.1	3700

[a] The functional form for the correlation function is $C(t) = \Delta_1^2 e^{-t/\tau_{c,1}} + \Delta_2^2 e^{-t/\tau_{c,2}} + \Delta_3^2 e^{-t/\tau_{c,3}}$.

is well described by a biexponential with a clear time scale separation into very fast and slow components. Previous 3PE and 2D IR spectroscopy of NMA-*d*/D_2O also predicted a correlation function with a time-scale separation between fast and slow processes, but treated these in the Bloch (instantaneous + static) limit.[18] In the other liquids, triexponentials were needed to adequately fit the 3PE data, reflecting a broader range of time scales in the amide I dephasing. The experimentally determined correlation functions are compared to those derived from MD simulations in Figure 7. Although there is not quantitative agreement in the amplitude and time scales, the two compare very well qualitatively, showing the same separation of time scales in the relaxation and similar overall behavior from one liquid to another. The results from simulation are well fit by biexponentials that are also summarized in Table 2.

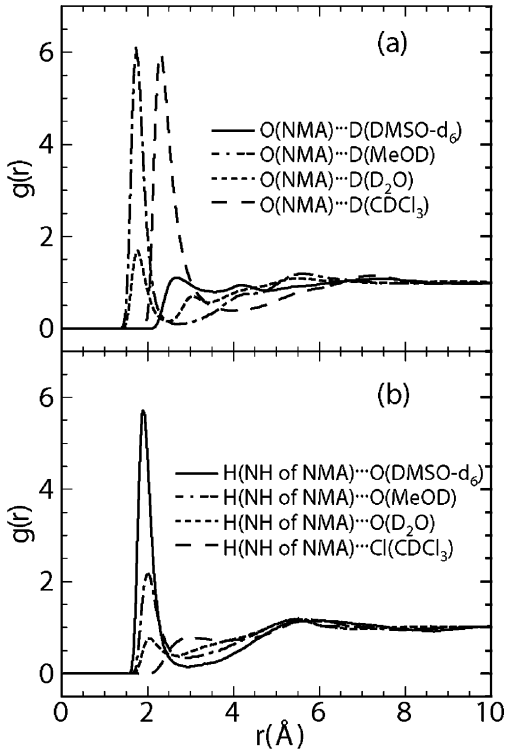

Figure 8. Radial distribution functions of various atoms of solvent molecules from (a) *O* atom of the NMA and (b) *H* atom of NH in the NMA.

D. Solvation Structure. We used the simulations to investigate local hydrogen bonding interactions in the various solvents. Figure 8a shows radial distribution functions $g(r)$ to various solvent atoms that can form hydrogen bonds or be involved in a similar electrostatic interaction with the NMA molecule. Specifically, we consider $g(r_{O\cdots D})$ for the separation of the *O* atom of NMA to the *D* atom of D_2O, *D* atom of OD in methanol, methyl *D* atom of DMSO-d_6, and *D* atom of $CDCl_3$. D_2O and methanol have a sharp first peak at the same distance of 1.7 Å, indicating that the hydrogen bond strengths of *O*(NMA) to these solvents are almost identical. In the case of NMA−$CDCl_3$, the first peak in the radial distribution function appears at 2.3 Å and is sharply peaked. On the other hand, the first peak in the case of NMA−DMSO is located at 2.7 Å and is less pronounced as expected for a less organized and non-hydrogen bonding configuration. On the basis of the observa-

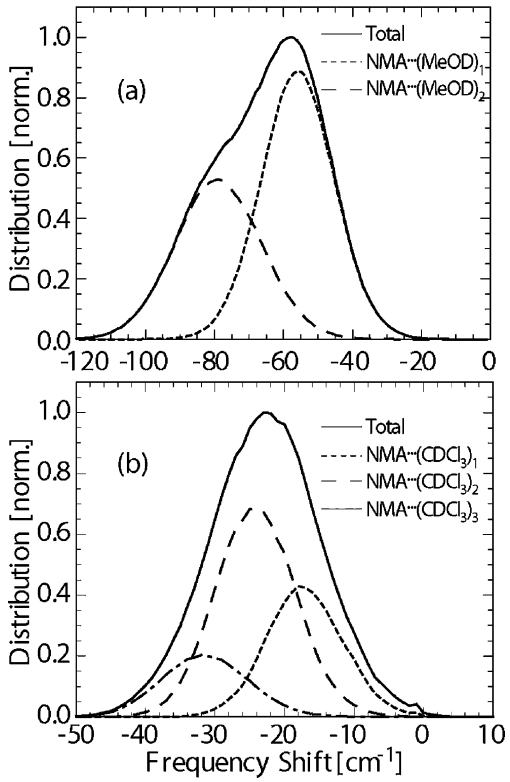

Figure 9. Probability distributions for amide I frequencies for configurations drawn from molecular dynamics simulations. (a) NMA in methanol showing singly (dotted) and doubly (dashed) hydrogen bonding configurations. (b) The distribution of the amide I mode frequency shift for the 4 ns MD simulation of the NMA−$CDCl_3$ system. The distributions for configurations with one (dotted), two (dashed), and three (dot−dash) $CDCl_3$ molecules are shown together with the total distribution (black).

tions in Figure 8a, the solvent $CDCl_3$ can form a weak hydrogen bond with the NMA carbonyl oxygen atom and this is the primary source of amide I mode frequency fluctuation.

Figure 8b shows the radial distribution functions $g(r_{H\cdots O})$ separating the *O* atom of D_2O, *O* atom of methanol, *O* atom of DMSO, and *C* atom of $CDCl_3$ from the *H* atom of NH in the NMA molecule. The peak positions are found at 1.88, 2.0, 2.0, and 2.98 Å for DMSO, D_2O, methanol, and $CDCl_3$, respectively. Therefore, it is observed that the NMA−DMSO system has the strongest hydrogen bond with *H* of NMA among the four solvents and the amide I mode frequency shift in the NMA−DMSO largely originates from the hydrogen bonding interaction of (DMSO)*O*···*H*−*N*(NMA).

E. NMA Hydrogen Bonding Dynamics in Methanol and $CDCl_3$. While a single Gaussian function accurately represents the fluctuating amide I frequency distribution of NMA in D_2O and DMSO-d_6, the asymmetric 2D line shapes of NMA-*d* in $CDCl_3$ (i.e. where the red side appears inhomogeneous while the blue side is homogeneous) indicate that the frequency band is non-Gaussian. This effect indicates an underlying structure to this transition that may have similarities to the case of NMA in methanol. Previous experiments[16] and molecular dynamics modeling[20] of 2D IR spectra of NMA in MeOD demonstrated that the two amide I resonances (seen in Figure 1) arose from multiple hydrogen bonding geometries and the kinetics of exchange between these configurations. Simulations were used to calculate the distribution of amide I frequency shifts for hydrogen bonding configurations from MD simulations (Figure 9a), which showed a distinct bimodal structure for NMA molecules with one or two hydrogen bonds to methanol. Direct modeling of the 2D IR spectra as a function of waiting time compares favorably with the experiment (Figure 6b), and reveals the 6 ps time scale for exchange between these environments as off-diagonal amplitude between the two peaks grows in.

To test whether a similar scenario exists in the NMA−$CDCl_3$ system, we separately calculated the distributions of the amide I mode frequency shifts with respect to the number of hydrogen bonds between the NMA and $CDCl_3$ molecules. Hydrogen bonds were defined as existing for O···D−C geometries between NMA and $CDCl_3$ such that $r_{O\cdots D} < 3.1$ Å and $\angle(O\cdots D-C) > 120°$. The distance criterion of 3.1 Å is determined from the corresponding radial distribution function in Figure 8a. Among 800 000 snapshot configurations extracted from the 4 ns MD trajectories, 25% correspond to cases when the NMA forms a single hydrogen bond with the $CDCl_3$ molecule. The populations of NMA hydrogen bonded with two and three $CDCl_3$ molecules are 53% and 19%, respectively, leaving virtually no non-hydrogen bonded species.

Figure 9b shows that the distribution of amide I frequency shift consists of three Gaussian distributions corresponding to the configurations with one, two, and three hydrogen bonds between the NMA and $CDCl_3$. Although the contribution from the configurations with two $CDCl_3$ molecules hydrogen bonded to the NMA is the largest, contributions from those with one and three $CDCl_3$ molecules hydrogen bonded to the NMA are significant and their different populations are likely to be the cause of non-Gaussian line shape of the IR absorption spectrum. In addition, it is believed that the asymmetric 2D line shapes of the NMA−$CDCl_3$ system shown in Figure 5c result from both of the following: there are multiple hydrogen bonded configurations in NMA−$CDCl_3$ solution and amide I frequency shift induced by the (NMA)O···D($CDCl_3$) interaction is rather small in comparison to that in the NMA−methanol system.

IV. Discussion

A. Hydrogen Bonding and Amide I Frequency. The effect of hydrogen bonding on NMA amide I absorption frequency has been noted for some time.[9−11] The correlated amide I red shift and increased line width in this series of solvents from DMSO to water is consistent with an increased strength of hydrogen bonding interaction between the solvent and the peptide unit.[63,64] Analogous to the spectroscopy of hydride stretches, this results from hydrogen bonding to the NMA oxygen that softens the anharmonic amide I potential. However, the amide I spectroscopy differs in that it is influenced by multiple hydrogen bonding sites to the NMA peptide unit. The presence of two distinct hydrogen bonding sites to NMA is most visible in methanol with two distinct peaks for singly and doubly hydrogen bonded configurations. Buck and Karplus first noted three hydrogen bonding sites for NMA/H_2O. While the interaction potential of a single H_2O favors a linear hydrogen bond,[60] the NMA oxygen is usually solvated by two waters.[19] These provide most of the amide I frequency shift from the gas phase, with hydrogen bonds from the N−H to water contributing less.[19] Our simulations indicate $CDCl_3$ preferentially solvates NMA with a close proximity between the O and D, also suggestive of a weak hydrogen bond. These observations argue that for the relatively weak hydrogen bonding interactions in this system, the effect of the solvent on amide I shift can be viewed as an electrostatic effect.

In addition to hydrogen bonding, a correlation of amide I frequency and solvent dielectric constant has previously been noted,[65] and a combination of hydrogen bonding and dielectric effect have been offered as an explanation for amide I intensities

in resonance Raman spectra.[59] It has been noted that water solvation induces an electronic polarization of NMA that contributes ~10% of the solvation energy.[66,67] If hydrogen bonding is viewed as a purely electrostatic effect then both short- and long-range Coulomb interactions should be expected to contribute to the frequency shift from the gas phase.

B. Correlation Functions and Line Shapes. The favorable qualitative comparison of the experimental and simulated correlation functions in Figures 3 and 7 indicates that the AMBER 7 intermolecular potential employed in the simulations is a fair representation of the liquid dynamics. The good comparison for the decay profiles of $C(t)$ indicates also that the correlation of amide I frequency and electrostatic potential captures the interactions between the amide I coordinate and the solvent. This offers additional evidence that both local and long-range electrostatic interactions contribute to the amide I frequency fluctuations. The relatively poor comparison of the line shape in $CDCl_3$ and DMSO obtained from simulation and experiment (Figure 1b) does not reflect the underlying dynamics, which enter into the correlation function. Rather, it reflects the parametrization of the strength of solute−solvent interaction, which will affect the overall amplitude of $C(t)$.

Qualitatively, the presence of picosecond and subpicosecond time scales in the experimental $C(t)$ reflects solvent relaxation processes expected for these liquids. Picosecond time scales are often attributed to diffusive relaxation and structural reorganization of these liquids. The subpicosecond time scales correspond to fluctuations about relatively fixed intermolecular configuration. These are particularly fast in D_2O, 50 fs librations, and 180 fs hydrogen bonding fluctuations,[68] and considerably slower librations in $CDCl_3$[69] and DMSO.[70]

At a more quantitative level, the time scales in our frequency correlation functions do not map simply onto solvent relaxation properties measured in other experiments. A comparison of the picosecond collective relaxation times studied by electronic solvation dynamics experiments,[71] optical Kerr effect,[70,72−74] and dielectric relaxation find a progressive lengthening in these time scales for H_2O, MeOH, $CHCl_3$, and DMSO, much like the long time $C(t)$ relaxation predicted from simulation.[75,76] Our experiments differ from these characterizations both in the relative long time relaxation rates from one liquid to another and in the absolute relaxation time scales. Previous experimental probes of the dynamics of these solvents are more sensitive to the collective effects and relaxation processes, i.e., the many body polarizability or dielectric response. Our measurements are clearly influenced strongly by the local nature of the hydrogen bonding interactions. Amide I vibrational dephasing as measured $C(t)$ is influenced both by the strength of the hydrogen bonding interaction and by the coupling of this local hydrogen bonding environment to collective reorganization of the liquid, which may exist on various time scales.

In the case of methanol, there is a time scale separation between fast fluctuations in hydrogen bond configurations and the kinetics of exchange between singly and doubly hydrogen bonded species. The relatively strong hydrogen bonds in this case have a pronounced effect on the amide I frequency shift. A probability distribution function for amide I frequencies obtained from snapshot MD configurations (Figure 9a) can be decomposed by the hydrogen bonding coordination of the NMA oxygen to either one or two methanol molecules. This reveals that the amide I frequency provides a reasonable discrimination of singly and doubly hydrogen bonded configurations, even though the static configurations suggest two overlapping distributions. The spectroscopy of these species differs somewhat because rapid fluctuations in the geometries of the two possible configurations narrow the distribution of frequencies, leading to distinct peaks in the linear and 2D IR spectra. The kinetics of exchange between the singly and doubly hydrogen bonded species occurs relatively slow on a ~6 ps time scale, leading to the growth of off-diagonal amplitude in the 2D IR spectra over picosecond waiting times (Figure 6).

For chloroform, similar effects are present but less apparent due to weak hydrogen bonding interactions and relatively slow dynamics in $CDCl_3$. As above, a decomposition of the amide I frequency probability distributions obtained in MD configurations reveals that between one and three chloroform molecules can coordinate with the NMA oxygen, although these distributions overlap significantly (Figure 9b). One cannot establish the stability of a solvation configuration merely from these static configurations; however, the spectral diffusion dynamics in the 2D IR spectra indicate that dynamics vary for species with different hydrogen bond coordination number out to picosecond time scales. In analogy to the case of methanol, it appears that we observe librational fluctuations within given configurations and longer time-scale exchange of coordination species. If the strength of the hydrogen bond in $CDCl_3$ does not depend on the number of H-bonded molecules, it is expected that the exchange between NMA−$(CDCl_3)_1$ and NMA−$(CDCl_3)_2$ is more frequent than the exchange between NMA−$(CDCl_3)_2$ and NMA−$(CDCl_3)_3$ on the basis of the relative distributions shown in Figure 9b. This observation may explain the preferential homogenization on the blue side of the 2D IR spectrum.

The form of the correlation function for NMA/D_2O is strikingly similar to that measured for the OH stretch vibrational frequency of HOD in D_2O. In the latter system, the vibrational frequency shifts are strongly influenced by hydrogen bonding to the solvent, and the form of the correlation function reflects the hydrogen bonding fluctuations and collective relaxation of D_2O.[26,68] In both systems, the similar form of the correlation function is a result of the same intermolecular D_2O dynamics being projected onto a high-frequency local vibrational coordinate. Our previous simulations of $C(t)$ for NMA/D_2O based on the electrostatic potential[19] and HOD/D_2O based on the electric field[26,27,41,77] give remarkably similar shapes. In a manner mirroring the empirical correlation of solvent electrostatic potential and amide I frequency, the OH frequency for HOD/D_2O was shown to originate in the molecular electric field of the D_2O solvent.[26] Due to its close proximity, the dominant source of this electric field is the hydrogen bonding partner, but a proper description of OH frequency must include the electric field over multiple solvent shells. Similarly, the short-range hydrogen bonding configuration will most strongly influence the NMA amide I frequency and its dynamics, whereas a full description must also include the longer range electrostatics.

Drawing on recent models of vibrational frequency shifts in hydrogen bonding liquids, we assign the solvation dynamics to fluctuating electric fields from the solvent acting on the amide I coordinate. These originate largely from librational, translational, and orientational dynamics of the solvent, but the intramolecular vibrations of the solvent can also contribute to the fastest time scales (as seen in the anisotropy measurements). The dominant source of these frequency fluctuations will be the closest charges, presumably the hydrogen bound protons (deuterons) of the solvent.

C. Electrostatics and Amide I Dephasing. The success of simulations based on electrostatic interactions demonstrates that the hydrogen bonding interactions and liquid dynamics are

accurately treated electrostatically for amide I frequency shifts. We now explore the origin of the frequency shift and the relationship between the electrostatic potential and electric field. Intermolecular forces that act on the amide I coordinate determine the time-varying amide I transition frequencies. Focusing on the amide I vibration only, one can describe the interaction of an amide I vibration with solvent degrees of freedom by Taylor-expanding interaction potential between the amide I coordinate and the solvent as

$$\tilde{H}_{\mathrm{SB}} = V_0 + \left(\frac{\partial V}{\partial \tilde{q}_i}\right)_{\mathrm{eq}} \tilde{q}_i + ... \approx V_0 + F_i \tilde{q}_i \qquad (11)$$

The first expansion term was explicitly written as[78]

$$F_i(t) = \sum_a \left\{ \left(\frac{\partial C_a}{\partial \tilde{q}_i}\right)_{\mathrm{eq}} \phi_a(t) + C_a \left(\frac{\partial \phi_a(t)}{\partial \tilde{q}_i}\right)_{\mathrm{eq}} \right\} \qquad (12)$$

where a denotes the sites of the NMA and C_a is the partial charge (or coarse-grained electron density) at site a. ϕ_a is the Coulombic electrostatic potential at the site a produced by the partial charges of the surrounding solvent molecules:

$$\phi_a(t) = \frac{1}{4\pi\epsilon_0} \sum_m \sum_j \frac{C_{j(m)}^{\mathrm{solvent}}}{r_{aj(m)}(t)} \qquad (13)$$

where $C_{j(m)}^{\mathrm{solvent}}$ denotes the partial charge of the jth site of the mth solvent molecule and they are assumed to be constants. $r_{aj(m)}$ is the distance between the NMA site a and the jth site of the mth solvent molecule. The linear force term in eq 11 induces structural distortion of the molecule along the anharmonic amide I coordinate in the presence of an external, spatially nonuniform electrostatic potential due to the partial charges of solvent molecules and it is responsible for vibrational dephasing.[80] The first term in eq 12 is determined not only by the electrostatic potential but also by the magnitudes of transition charges, whereas the second term is determined by the gradient of the electrostatic potential. The latter is related to the electric field, spatial gradient of the potential. As discussed in ref 78, the contribution from the first term is larger than that from the second term.

It is prohibitively difficult to accurately calculate the values of $(\partial C_a/\partial \tilde{q}_i)_{\mathrm{eq}}$ representing the response of charge distributions upon the electrostatic interaction between solute and solvent molecules due to the polarizable nature of molecules. Still those who are familiar with gas-phase ab initio geometry optimizations might wonder why it is difficult to calculate quantities such as $(\partial C_a/\partial \tilde{q}_i)_{\mathrm{eq}}$. The key aspect behind this complication is because the gas-phase molecular structure of NMA differs from the ensemble-averaged, equilibrium molecular geometry of the NMA in solution. Consequently, the linear derivatives, $(\partial C_a/\partial \tilde{q}_i)_{\mathrm{eq}}$, should be taken at the ensemble-averaged NMA structure in solution not at the geometry-optimized NMA structure in a gas-phase—note that the conventional approach based on modeling intermolecular interactions by extrapolating the isolated gas-phase molecule properties fails in this case. Second, the eigenvector elements of the amide I vibrational mode for an isolated NMA in the Cartesian coordinate system differ from those of the solvated NMA. Therefore, the present approach used in this paper is (i) to approximate eq 11 as $F_i = \sum_a x_a \phi_a$, where the values of x_a are variational parameters as discussed in ref 14, (ii) to use an ensemble of NMA−solvent molecule clusters instead of the ab initio calculation results for a single isolated NMA, and (iii) to determine parameters l_a depending also on the potential anharmonicity of the ensemble-averaged NMA molecule in solution by fitting to quantum chemistry calculation results for various NMA−water clusters.

The recent study of Skinner and co-workers[31] also considered various clusters and used the ab initio calculation results, but it was based on the assumption that the second term in eq 11 becomes the dominant factor. Furthermore, the C_a values were essentially considered to be adjusted parameters accommodating the effects of the neglected first term. Their results for the NMAD−D_2O system are comparable to those of the present approach, but the magnitude of amide I frequency shift is about 15% smaller in comparison with that of the present approach. It is believed that this discrepancy results mainly from the fact that at large distances the electric field decays faster than the electrostatic potential.

D. Vibrational Lifetime. The present measurements of amide I vibrational relaxation in NMA indicates that is not a simple process. Our ad hoc treatment of population relaxation in the modeling of the spectroscopy draws on traditional two state relaxation. The origin of the observed biexponential decay is still unclear, but it certainly involves more than two vibrational states. It is possible that there is rapid femtosecond exchange between amide I $\upsilon = 1$ and another dark state followed by picosecond relaxation to $\upsilon = 0$. A similar time scale separation in the relaxation was observed in acetylproline, but also not assigned, although relaxation to amide II was ruled out.[35,79] Also it is unclear what the role of the solvent is, whether the change in fast and slow relaxation is a function of coupling to the solvent or merely peptide deuteration influencing intramolecular couplings. Initial work to computationally investigate amide I vibrational energy relaxation of NMA in D_2O was reported by Nguyen and Stock.[80] With use of instantaneous normal-mode analysis of MD simulations of a flexible empirical potential, it was found mixing of the CO stretch with other vibrations of NMA was appreciable, and that the classical fluctuating force acting on the amide I coordinate considerably underestimated the relaxation rate.

The origin of vibrational population relaxation processes in NMA remains a mystery that will require further investigations into inter- and intramolecular relaxation pathways. Even now, there seems to be some inconsistency between our relaxation times and others that have been reported for NMA/D_2O.[18,34] Such studies remain important to understanding the vibrational spectroscopy of peptides and proteins, since these relaxation processes dominate the vibrational line width. Our results indicate that the anharmonic peptide potential probably involves relatively strong mixing of amide I and other backbone states. Such studies may also be able to explain why the amide I lifetime in myoglobin is mostly temperature independent—indeed it gets somewhat faster as the temperature is lowered.[81]

V. Summary and Conclusions

In this article, we have retrieved the frequency−frequency correlation function of the amide I transition for the isolated peptide unit of NMA in polar solvents. Three model solvents, which represent different hydrogen bonding geometries, varying strength of solute−solvent interaction, and a different time scale of solvent motion, reveal the effect of local interactions and electrostatics on the peptide unit. Strong hydrogen bonding solvents with fast fluctuations, such as water, cause vibrational dephasing on a time scale of less than 1 ps, whereas the weaker, slower solvents cause dephasing on a several picosecond time scale. Comparisons to molecular dynamics simulations indicate

that the frequency fluctuations are well described in terms of electrostatic interactions between the solvent and amide I coordinate. The variation of the electrostatic potential along the amide I coordinate originating in the solvent molecules is an electric field that correlates strongly with vibrational frequency. This observation should greatly simplify the assignment of amide I site energies in calculations of the amide I spectroscopy of larger peptides and proteins.

Acknowledgment. We would like to thank Munira Khalil and Nuri Demirdöven for technical assistance. A.T. acknowledges support from the Basic Energy Sciences of the U.S. Department of Energy (DE-FG02-99ER14988), the National Science Foundation (U.S.A; Grant CHE-0316736), and the Petroleum Research Fund, administered by the American Chemical Society. A.T. thanks the Alfred P. Sloan Foundation and the David and Lucile Packard Foundation for their fellowship support. M.C. is grateful for financial support from the KOSEF (CRIP), Korea.

References and Notes

(1) Krimm, S.; Bandekar, J. *Adv. Protein Chem.* **1986**, *38*, 181.
(2) Barth, A.; Zscherp, C. *Q. Rev. Biophys.* **2002**, *35*, 369.
(3) Woutersen, S.; Hamm, P. *J. Phys.*: *Condens. Matter* **2002**, *14*, R1035.
(4) Hamm, P.; Lim, M.; Hochstrasser, R. M. *J. Phys. Chem. B* **1998**, *102*, 6123.
(5) Hamm, P.; Hochstrasser, R. M. In *Ultrafast Infrared and Raman Spectroscopy*; Fayer, M. D., Ed.; Marcel Dekker: New York, 2001; p 273.
(6) Gnanakaran, S.; Hochstrasser, R. M. *J. Am. Chem. Soc.* **2001**, *123*, 12886.
(7) Woutersen, S.; Hamm, P. *J. Chem. Phys.* **2001**, *114*, 2727.
(8) Woutersen, S.; Mu, Y.; Stock, G.; Hamm, P. *Proc. Natl. Acad. Sci.* **2001**, *98*, 11254.
(9) Mirkin, N. G.; Krimm, S. *J. Am. Chem. Soc.* **1991**, *113*, 9742.
(10) Mirkin, N. G.; Krimm, S. *J. Mol. Struct.* **1996**, *377*, 219.
(11) Torii, H.; Tatsumi, T.; Kanazawa, T.; Tasumi, M. *J. Phys. Chem. B* **1998**, *102*, 309.
(12) Herrebout, W. A.; Clou, K.; Desseyn, H. O. *J. Phys. Chem. A* **2001**, *105*, 4865.
(13) Kubelka, J.; Keideling, T. A. *J. Phys. Chem. A* **2001**, *105*, 10922.
(14) Ham, S.; Kim, J.-H.; Lee, H.; Cho, M. *J. Chem. Phys.* **2003**, *118*, 3491.
(15) Ham, S.; Cho, M. *J. Chem. Phys.* **2003**, *118*, 6915.
(16) Woutersen, S.; Mu, Y.; Stock, G.; Hamm, P. *Chem. Phys.* **2001**, *266*, 137.
(17) Woutersen, S.; Pfister, R.; Hamm, P.; Mu, Y. G.; Kosov, D. S.; Stock, G. *J. Chem. Phys.* **2002**, *117*, 6833.
(18) Zanni, M. T.; Asplund, M. C.; Hochstrasser, R. M. *J. Chem. Phys.* **2001**, *114*, 4579.
(19) Kwac, K.; Cho, M. *J. Chem. Phys.* **2003**, *119*, 2247.
(20) Kwac, K.; Lee, H.; Cho, M. *J. Chem. Phys.* **2004**, *120*, 1477.
(21) Eaton, G.; Symons, M. C. R. *J. Chem. Soc., Faraday Trans.* **1991**, *85*, 3257.
(22) Scheurer, C.; Piryatinski, A.; Mukamel, S. *J. Am. Chem. Soc.* **2001**, *123*, 3114.
(23) Rey, R.; Hynes, J. T. *J. Chem. Phys.* **1996**, *104*, 2356.
(24) Rey, R.; Hynes, J. T. *J. Chem. Phys.* **1998**, *108*, 142.
(25) Rey, R.; Moller, K. B.; Hynes, J. T. *Chem. Rev.* **2004**, *104*, 1915.
(26) Fecko, C. J.; Eaves, J. D.; Loparo, J. J.; Tokmakoff, A.; Geissler, P. L. *Science* **2003**, *301*, 1698.
(27) Eaves, J. D.; Tokmakoff, A.; Geissler, P. *J. Phys. Chem. B.* In preparation.
(28) Kwac, K.; Cho, M. *J. Chem. Phys.* **2003**, *119*, 2256.
(29) Williams, R. B.; Loring, R. F.; Fayer, M. D. *J. Phys. Chem. B* **2001**, *105*, 4068.
(30) Merchant, K. A.; Noid, W. G.; Akiyama, R.; Finkelstein, I. J.; Goun, A.; McClain, B. L.; Loring, R. F.; Fayer, M. D. *J. Am. Chem. Soc.* **2003**, *125*, 13804.
(31) Schmidt, J. R.; Corcelli, S. A.; Skinner, J. L. *J. Chem. Phys.* **2004**, *121*, 8887.
(32) Bour, P.; Keideling, T. A. *J. Chem. Phys.* **2003**, *119*, 11253.
(33) Bour, P. *J. Chem. Phys.* **2004**, *121*, 7545.
(34) Hamm, P.; Lim, M.; Hochstrasser, R. M. *J. Phys. Chem. B* **1998**, *102*, 6123.
(35) Rubtsov, I. V.; Hochstrasser, R. M. *J. Phys. Chem. B* **2002**, *106*, 9165.
(36) Bredenbeck, J.; Hamm, P. *J. Chem. Phys.* **2003**, *119*, 1569.
(37) Chen, X. G.; Schweitzer-Stenner, R.; Krimm, S.; Mirkin, N. G.; Asher, S. A. *J. Am. Chem. Soc.* **1994**, *116*, 1141.
(38) Kim, J.-H.; Cho, M. *Bull. Korean Chem. Soc.* **2003**, *24*, 1061.
(39) Fecko, C. J.; Loparo, J. J.; Roberts, S. T.; Tokmakoff, A. *J. Chem. Phys.* **2004**, in press.
(40) Asbury, J. B.; Steinel, T.; Stromberg, C.; Corcelli, S. A.; Lawrence, C. P.; Skinner, J. L.; Fayer, M. D. *J. Phys. Chem. A* **2004**, *108*, 1107.
(41) Corcelli, S. A.; Lawrence, C. P.; Skinner, J. L. *J. Chem. Phys.* **2004**, *120*, 8107.
(42) Woutersen, S.; Hamm, P. *J. Chem. Phys.* **2001**, *115*, 7737.
(43) de Boeij, W. P.; Pshenichnikov, M. S.; Wiersma, D. A. *Chem. Phys.* **1998**, *233*, 287.
(44) Everitt, K. F.; Geva, E.; Skinner, J. *J. Chem. Phys.* **2001**, *114*, 1326.
(45) Piryatinski, A.; Skinner, J. L. *J. Phys. Chem. B* **2002**, *106*, 8055.
(46) Tokmakoff, A. *J. Phys. Chem. A* **2000**, *104*, 4247.
(47) Khalil, M.; Demirdöven, N.; Tokmakoff, A. *J. Phys. Chem. A* **2003**, *107*, 5258.
(48) Golonzka, O.; Khalil, M.; Demirdöven, N.; Tokmakoff, A. *J. Chem. Phys.* **2001**, *115*, 10814.
(49) Fleming, G. R.; Cho, M. *Annu. Rev. Phys. Chem.* **1996**, *47*, 109.
(50) Chung, H. S.; Khalil, M.; Tokmakoff, A. *J. Phys. Chem. B* **2004**, *108*, 15332.
(51) Ohta, K.; Maekawa, H.; Tominaga, K. *J. Phys. Chem. A* **2004**, *108*, 1333.
(52) Sung, J.; Silbey, R. J. *J. Chem. Phys.* **2001**, *115*, 9266.
(53) Cho, M. *J. Chem. Phys.* **2001**, *115*, 4424.
(54) Tokmakoff, A. *J. Chem. Phys.* **1996**, *105*, 1.
(55) Wang, J. M.; Cieplak, P.; Kollman, P. A. *J. Comput. Chem.* **2000**, *21*, 1049.
(56) Cornell, W. D.; Cieplak, P.; Bayly, C. I.; Gould, I. R.; Merz, K. M.; Ferguson, D. M.; Spellmeyer, D. C.; Fox, T.; Caldwell, J. W.; Kollman, P. A. *J. Am. Chem. Soc.* **1995**, *117*, 5179.
(57) Darden, T.; York, D.; Pedersen, L. *J. Chem. Phys.* **1993**, *98*, 10089.
(58) Berendsen, H. J. C.; Postma, J. P. M.; Vangunsteren, W. F.; Dinola, A.; Haak, J. R. *J. Chem. Phys.* **1984**, *81*, 3684.
(59) Mayne, L. C.; Hudson, B. *J. Phys. Chem.* **1991**, *95*, 2962.
(60) Buck, M.; Karplus, M. *J. Phys. Chem.* **2001**, *105*, 11000.
(61) Köddermann, T.; Ludwig, R. *Phys. Chem. Chem. Phys.* **2004**, *6*, 1867.
(62) Joo, T.; Jia, Y.; Yu, J.-Y.; Lang, M. J.; Fleming, G. R. *J. Chem. Phys.* **1996**, *104*, 6089.
(63) Pimentel, G. C.; McClellan, A. L. *The Hydrogen Bond*; Freeman: San Francisco, CA, 1960.
(64) Nibbering, E. T. J.; Elsaesser, T. *Chem. Rev.* **2004**, *104*, 1887.
(65) Torii, H.; Tasumi, M. *J. Raman Spectrosc.* **1998**, *29*, 537.
(66) Ding, Y.; Bernardo, D. N.; Krogh-Jespersen, K.; Levy, R. M. *J. Phys. Chem.* **1995**, *99*, 11575.
(67) Gao, J.; Freindorf, M. *J. Phys. Chem. A* **1997**, *101*, 3182.
(68) Loparo, J. J.; Fecko, C. J.; Eaves, J. D.; Roberts, S. T.; Tokmakoff, A. *Phys. Rev. B* **2004**, *70*, 180201.
(69) McMorrow, D.; Lotshaw, W. T.; Kenney-Wallace, G. A. *IEEE J. Quantum Electron.* **1988**, *QE-24*, 443.
(70) Wiewior, P. P.; Shirota, H.; Castner, E. W. *J. Chem. Phys.* **2002**, *116*, 4643.
(71) Lang, M. J.; Jordanides, X. J.; Song, X.; Fleming, G. R. *J. Chem. Phys.* **1999**, *110*, 5884.
(72) Fecko, C. J.; Eaves, J. D.; Tokmakoff, A. *J. Chem. Phys.* **2002**, *117*, 1139.
(73) Castner, E. W., Jr.; Chang, Y. J.; Chu, Y. C.; Walrafen, G. E. *J. Chem. Phys.* **1995**, *102*, 653.
(74) Loughnane, B. J.; Scodinu, A.; Farrer, R.; Fourkas, J. T.; Mohanty, U. *J. Chem. Phys.* **1999**, *111*, 2686.
(75) Castner, E. W.; Maroncelli, M. *J. Mol. Liq.* **1998**, *77*, 1.
(76) Horng, M. L.; Gardecki, A.; Papuzayan, A.; Maroncelli, M. *J. Phys. Chem.* **1995**, *99*, 17311.
(77) Hayashi, T.; Jansen, T. l. C.; Zhuang, W.; Mukamel, S. *J. Phys. Chem. A* **2005**, *109*, 64.
(78) Cho, M. *J. Chem. Phys.* **2003**, *118*, 3480.
(79) Rubtsov, I. V.; Wang, J.; Hochstrasser, R. M. *Proc. Natl. Acad. Sci. U.S.A.* **2003**, *100*, 5601.
(80) Nguyen, P. H.; Stock, G. *J. Chem. Phys.* **2003**, *119*, 11350.
(81) Peterson, K. A.; Rella, C. W.; Engholm, J. R.; Schwettman, H. A. *J. Phys. Chem. B* **1999**, *103*, 557.